Cumhuriyet Sci. J., 46(1) (2025) 79-90
DOI: https://doi.org/10.17776/csj.1548916

Cumhuriyet Science Journal

| csj.cumhuriyet.edu.tr | Founded: 2002 ISSN: 2587-2680 e-ISSN: 2587-246X Publisher: Sivas Cumhuriyet University

Exploring the Impacts of Substitution Position on Structural, Electronic, and Energetic Characteristics of Selected Chalcone Derivatives by DFT Method: A Quantum Computational Research

Sümeyya Serin [1,a,*]

[1] *Inonu University, Scientific and Technological Research Center, 44280, Malatya, Türkiye*

**Corresponding author*

Research Article

History
Received: 12/09/2024
Accepted: 12/02/2025

ABSTRACT

Chalcone derivatives are frequently utilized as a versatile scaffold in molecular design studies due to their broad-spectrum activities. Structural modification studies applied to increase their biological activities to a remarkable level reveal the importance of substitution positions on aromatic rings. In this respect, the study aimed to explore the effects of changing substitution positions on molecular properties. Herein, the effects of distinct substitution positions on thermodynamic and physicochemical parameters, reactivity descriptors, absorption characteristics, and intramolecular interactions were investigated utilizing quantum chemical methods. To this end, (Density Functional Theory) DFT-based calculations were performed using the GAUSSIAN 16 software with B3LYP/6-311++G (d, p) level on *ortho*-OH, *meta*-OH, and *para*-OH substituted chalcone derivatives. While the calculated dipole moment and polarizability values differ, very similar results were obtained for the ΔE (total energy), ΔH (enthalpy), and ΔG (Gibbs free energy) parameters. The highest polarizability value, 296.193 a.u., was obtained for the *para*- isomer. The ΔE_g values in the gas phase were calculated as: 4.013 eV (*m*-) > 3.898 eV (*p*-) > 3.832 eV (*o*-). Also, the effects of different solvents on the absorption spectra of the studied isomers were investigated theoretically using (Time Dependent) TD-DFT calculations. Molecular orbitals contributing to electronic transitions were determined for each phase. It is further anticipated that the research findings will offer novel insights to inform future studies on the implications of the substitution position.

Keywords: Chalcone, Substitution position, DFT, Reactivity, Absorption characteristics

[a] *sumeyya.alatas@inonu.edu.tr* *https://orcid.org/0000-0002-4637-1734*

Introduction

Chalcones are plant-derived polyphenolic compounds belonging to the flavonoids family. They have been the subject of numerous studies due to their bioactive nature. Therapeutical applications of chalcone derivatives date back to when plants were utilized in order to treat distinct medical disorders [1]. Over time, research on the design, synthesis and determination of application areas of more specific derivatives has increased. Studies on determining various pharmacological activities such as anticancer [2], antioxidant [3], anti-inflammatory [4], anticonvulsant [5], and antifungal [6] have been frequently encountered in the literature. The typical scaffold in chalcones is the most investigated structure for potential anticancer activity. In particular, hydroxy-substituted chalcones have been demonstrated to exhibit activity as cytotoxic and tumor-reducing agents [7]. Some well-known natural chalcones that are used in pharmaceuticals include isoliquiritigenin, butein, and isobavachalcone (Figure 1.). Modifying the chemical structures of chalcones allowed the examination of their structure-activity relationships to improve pharmacological activity. The types, numbers and positions of substituents have been effective in the preparation of structurally diverse chalcone derivatives. In a study conducted by Ma et al., a series of hydroxychalcone derivatives were synthesized and appraised for their in vitro inhibitory activities of β-secretase (BACE1) [8]. If we characterize the two phenyl groups in the structure of chalcone as PhC=O and PhC-H, the relevant study focused on how the position of a hydroxyl group in the PhC-H ring affects the inhibitor activity. IC_{50} values of 2.45 ± 0.39 µM, 8.03 ± 0.92 µM, and 33.00 ± 3.75 µM were obtained for *ortho*, *meta*, and *para* substitution, respectively. Therefore, it was determined that the *ortho* position was more effective than other substitution positions. In a recent study by Cyboran-Mikołajczyk et al., the relationship between the biological activities and chemical structure of compounds containing a chloro substituent at various positions of the PhC=O and PhC-H rings of chalcone was investigated, as well as their effects on membranes, cancer cells and bacterial cells [9]. Within the scope of the study, five different 2'-hydroxychalcone derivatives with chlorine atoms in various positions were synthesized. While the chlorine substituent increases the lipophilic character of 2'-hydroxychalcone, the highest n-octanol/water partition coefficient ($logP_{ow}$) of 2.90 was obtained for 2-chloro-2'-hydroxychalcone derivative. Higher lipophilicity value indicates easier membrane permeation. The ability of the derivatives to inhibit bacterial growth and biofilm

formation varies based on the substitution positions in the phenyl rings. Another study carried out by Patil and Zangade focused on the synthesis and anticancer activities of chalconoid based Co (II) complexes with 2-hydroxychalcones containing naphthalene moiety [10]. The anticancer activities of six synthesized complexes were evaluated against the liver cancer cell line (Hep G2). The findings of the study revealed that the complex having –OH substituent at *meta-para* position of PhC-H ring exhibited considerable activity with IC_{50} value of 64.21 µg/mL. In their previously published study, Bronikowska et al. investigated the effects of *ortho*-, *meta*- and *para*-methoxy derivatives of 2'-hydroxychalcones on the release of IL-8, MIF, VCAM-1, ICAM-1 by colon cancer SW480 and SW620 cell lines [11]. Test results revealed that the studied methoxy derivatives exhibited modulating effect on colon cancer cells. Besides, it was reported that *meta*-methoxy derivative at the concentration of 25 µM considerably decreased IL-8 secreted by SW480 and SW620 cancer cells. In another study conducted by Wilhelm et al., cytotoxicity evaluation was carried out on four chalcone derivatives in which the substitution positions and substituents differed [12]. Cytotoxic activity examination was performed in vitro in various cancer cell lines, including breast adenocarcinoma (MCF7), T-lymphoblastic leukemia (CEM), cervical carcinoma (HeLa) lines, malignant melanoma (G-361), and skin fibroblasts (BJ). It has been reported that the best activity was observed against CEM cells. IC_{50} values obtained in the study revealed that the presence of the hydroxy group on the PhC-H ring has a prominent influence on cytotoxicity. Furthermore, one of the important findings emphasized in the study is that *para*-OH substitution exhibited high cytotoxicity and selectivity.

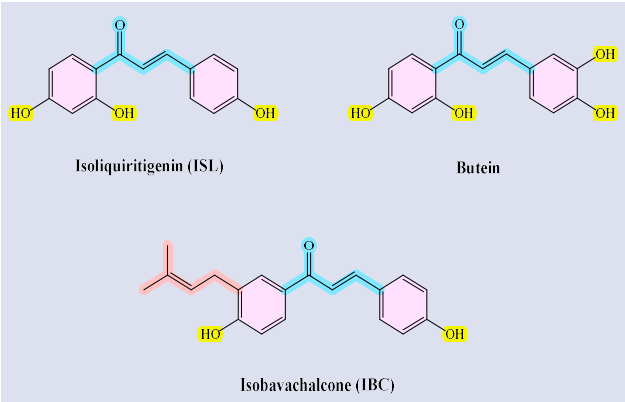

Figure 1. Structures of some naturally derived chalcones.

Keeping these considerations in mind, it is concluded that the bioactivity potential of chalcones is affected by the substitution positions of the substituents on the PhC=O and PhC-H aromatic rings. Therefore, it has becoming more substantial to explore the impacts of positional isomerism on molecules. The use of computational techniques in this laborious exploration duration provides a great advantage to researchers as it ensures the opportunity to evaluate various characteristics of the molecules of interest both numerically and visually [13]. DFT is one of the most versatile techniques available to examine the ground state properties of various molecular systems, especially electronic characteristics. By offering less computational time, excellent accuracy, and being cost-effective compared to other methods, DFT computations remain popular among computational chemists [14]. The theoretical investigation of how the relative position of the substituents affects to the molecular properties motivated this study. Herein, quantum chemical calculations were conducted in three different solvent environments (acetonitrile, DMSO, and water) by selecting *ortho*, *meta*, and *para*-OH substituted chalcone derivatives. The effects of both substituent position and solvent environment on the physicochemical, electronic and molecular properties of OH-substituted chalcone derivatives were examined from a theoretical perspective. A preliminary study of the solvent and/or substituent position effect provides insight into subsequent phase studies. The observation that interaction forces in solution are significantly more pronounced and diversified compared to those in the gas phase enables the modulation of solute properties and reactivities across a range of processes. It is expected that the research findings will provide new perspectives for future studies on the effects of the substitution position.

Computational Methodology

All DFT computations operated in this work were performed by using GAUSSIAN 16 software package [15] with B3LYP hybrid functional and the 6-311++G (d, p) basis [16-18]. Gauss View 6 software [19] was utilized for visualizations of the optimized structure, FMOs, and MEP diagrams. To gain the density of states (DOS) plot, Gauss-Sum 3.0 [20] program was utilized. The solvent phase (acetonitrile, ACN (ε=35.7), DMSO (*ε*=46.8), and water (*ε*=78.4)) simulations were carried out by using Integral Equation Formalism Polarizable Continuum Model (IEFPCM) [21]. For computations, optimized structure was verified by the absence of imaginary frequency. The TD-DFT method [22] was utilized to enlighten UV–vis. features such as possible electronic transitions, energies, and oscillator strengths.

The thermochemical quantities, $E_{vib.}$ (vibrational thermal energy), $S_{vib.}$ (vibrational entropy), and $Cv_{vib.}$ (vibrational heat capacity) values were calculated through specific equations ((1)-(5)) defined below in accordance with the principles of quantum mechanics [23-25]. The following explanations refer to the terms presented in the equations: $\Theta_{v,j}=hvj\ /k$ →vibrational temperature, k→ Boltzmann constant, h→ Planck constant, and vj→ j^{th} fundamental frequency.

$$Q = Q_{trans.} \times Q_{rot.} \times Q_{vib.}\, Q_{elec.} \quad (1)$$

$$Q_{vib.} = \prod_{j=1}^{3N-6} \frac{e^{-\Theta_{v,j}/2T}}{\left(1 - e^{-\frac{\Theta_{v,j}}{T}}\right)} \quad (2)$$

$$E_{vib.} = Nk \sum_{j=1}^{3N-6} \left(\frac{\Theta_{v,j}}{2} + \frac{\Theta_{v,j}\, e^{-\Theta_{v,j}/T}}{\left(1 - e^{-\frac{\Theta_{v,j}}{T}}\right)} \right) \quad (3)$$

$$S_{vib.} = Nk \sum_{j=1}^{3N-6} \left[\frac{\Theta_{v,j}/T}{\left(e^{\Theta_{v,j}/T} - 1\right)} - ln\left(1 - e^{-\Theta_{v,j}/T}\right) \right] \quad (4)$$

$$Cv_{vib.} = Nk \sum_{j=1}^{3N-6} \left[\left(\frac{\Theta_{v,j}}{T}\right)^2 \frac{e^{\Theta_{v,j}/T}}{\left(e^{\Theta_{v,j}/T} - 1\right)^2} \right] \quad (5)$$

According to Koopmans theorem [26], ionization energy (I) (I= - E_{HOMO}) and electron affinity (A) (A= -E_{LUMO}) values can be defined by HOMO (Highest Occupied Molecular Orbital) and LUMO (Lowest Unoccupied Molecular Orbital) energies. Additionally, some quantum chemical reactivity parameters, calculated utilizing I and A values, with their corresponding equations are presented below (6-13) [27-33].

$$\text{Chemical Potential } \mu = -\frac{I + A}{2} \quad (6)$$

$$\text{Chemical Hardness } \eta = \frac{I - A}{2} \quad (7)$$

$$\text{Electronegativity } \chi = \frac{I + A}{2} \quad (8)$$

$$\text{Electrophilicity Index } \omega = \frac{\mu^2}{2\eta} \quad (9)$$

$$\text{Electron-Accepting Power } \omega^+ \approx (I + 3A)^2/(16(I - A)) \quad (10)$$

$$\text{Electron-Donating Power } \omega^- \approx (3I + A)^2/(16(I - A)) \quad (11)$$

$$\text{Maximum Charge Transfer Capability } \Delta N_{max} = \frac{I + A}{2(I - A)} \quad (12)$$

$$\text{Back-Donation Energy } \Delta\varepsilon_{back-donatio} = -\frac{\eta}{4} \quad (13)$$

NBO (Natural Bond Orbitals) analysis of studied compounds were also performed utilizing the 2nd-order Fock matrix [34-35] at B3LYP/6–311++G (d, p) theory level. Thus, possible donor-acceptor orbital interactions and corresponding stabilization energy predictions were noted. Stabilization energy values were calculated according to the formula specified in equation (14). The terms in the formula are expressed as follows: $E^{(2)}$: Stabilization energy, *qi*: Donor orbital occupancy, *Fij:* Off diagonal Fock matrix, *εi* and *εj*: diagonal element, donor and acceptor orbital energies.

$$E^{(2)} = \Delta E_{ij} = qi\left[\frac{(Fij)^2}{(\varepsilon j - \varepsilon i)}\right] \quad (14)$$

Results and Discussion

PES (Potential energy Surfaces) Scan Analysis and Molecular Structure

The investigated chalcone derivatives were optimized in the gaseous state using B3LYP/6- 311++G (d, p) level. X-Ray structures were employed for optimization of *meta*- and *para*- derivatives [12]. The crystal structures were ensured from the Cambridge Crystallographic Data Center (CCDC 2062760 for *m*-OH and 2062757 for *p*-OH) [12]. The resulting DFT-optimized geometries have been represented in Figure 2 ((B) and (C)). In order to evaluate the compatibility of the X-ray structures and the DFT-optimized structures, atom-by-atom superimposition was performed (Figure 3). RMSD is a crucial metric in scientific research, utilized in a variety of ways. It is employed to ascertain the stability of protein-ligand complexes during molecular dynamics simulations, to compare the structural similarity between crystallized and modeled frameworks, and to evaluate the mean change in motion of selected atoms during simulations [36]. The root mean square deviation (RMSD) values were determined as 0.607 Å for *m*-OH isomer and 0.221 Å for *p*-OH isomer. These values are indicative of a satisfactory level of distinction between the structures, suggesting that the observed differences are within an acceptable range. However, since no X-ray structure is available for the ortho isomer, to assign the most stable geometry, conformational analysis has been achieved by operating B3LYP/ 6-311++G (d, p) methodology. The PES computations were carried out in accordance with C14-C4-C2-C5 and C5-C3-C23-27 dihedral angles. The PES scan analysis was conducted by altering the dihedral angles at each step by 10˚ along the specified bond axis. The "Scan of Total Energy" diagrams obtained as a result of the analysis are displayed in Figure 4. The minima (steps 21 and 20) and maxima (steps 29 and 8) points obtained by the rotation of the selected dihedral angles are shown on the diagram. According to PES analysis results, it is revealed that the C14-C4-C2-C5 and C5-C3-C23-27 dihedral angles have rotational potential barrier values of 4.77 and 3.70 kcal/mol. Therefore, the highest value for the energy difference between the most stable conformer and the most unstable conformer was detected in the C14-C4-C2-C5 dihedral angle scan. Namely, minimum energy and improved stability were monitored when rotating round the C14-C4-C2-C5 dihedral angle. Consequently, the lowest energy structure obtained from the relevant dihedral angle scan was used as the basis for further calculations. The DFT-optimized structure of the *ortho* isomer is shown in Figure 2 (A).

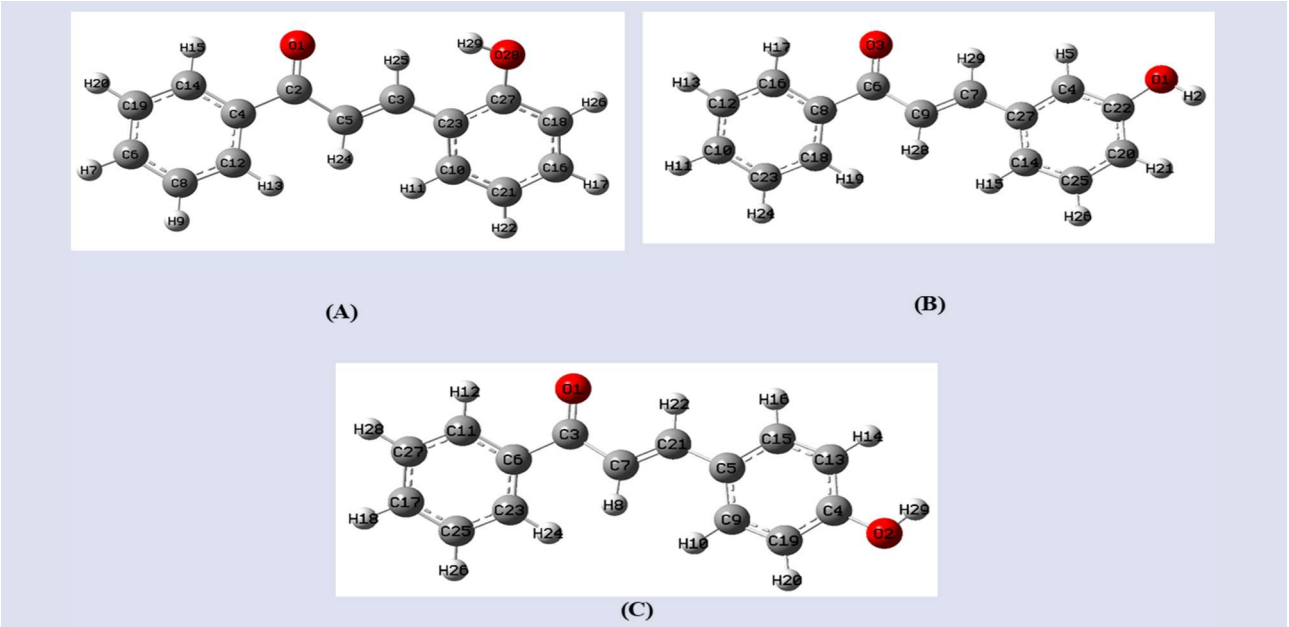

Figure 2. DFT-optimized structures of *o*-OH (A), *m*-OH (B), and *p*-OH (C) derivatives with atomic numbering scheme.

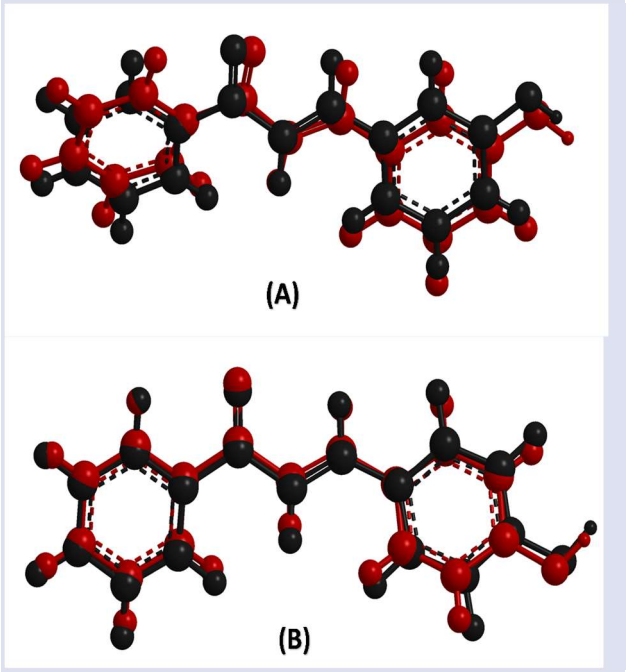

Figure 3. Atom-by-atom superimposition of the DFT-optimized structures (black) and the X-ray structures (red) for *m*-OH (A) and *p*-OH (B) isomers.

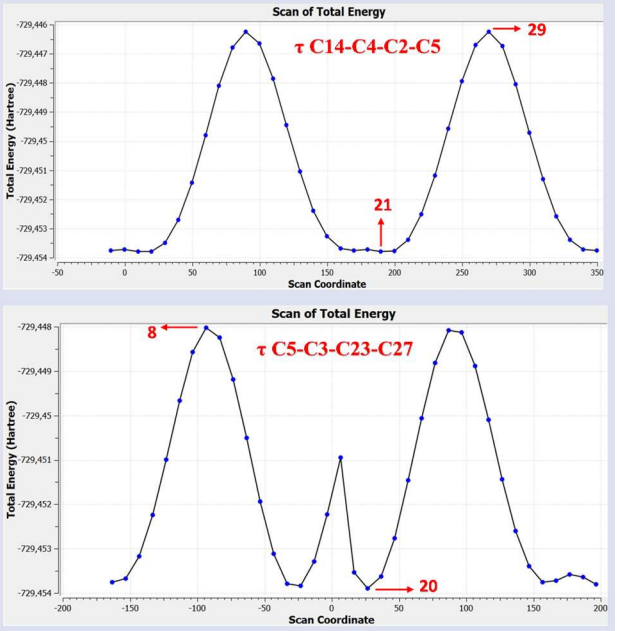

Figure 4. Potential energy surfaces scan of *o*-OH substituted isomer

Some of selected bond lengths (Å), bond angles (°), and dihedral angles (°) are listed in Table 1. From Table 1, it is observed that the C=O carbonyl bond lengths of *ortho-*, *meta-,* and *para-* derivatives were calculated as 1.225 Å, 1.223 Å, and 1.225 Å, respectively. The experimental value for the relevant bond length was determined as 1.237 Å. In the case of aromatic ring C-C bond lengths, they were computed in the range of 1.401-1.414 Å for all three compounds. Experimental C-C distances have been reported in the range of 1.385-1.398 Å. The O1-C2-C5 and O1-C2-C4 bond angles of the *ortho-* derivative were estimated as 121.09° and 119.99° respectively.

The equivalents of these angles in *meta-* and *para-*derivatives were calculated as 121.36°/119.89° and 121.57°/119.72°, respectively. Therefore, it is evident that values close to the experimental data (120.40° /119.33°) are obtained. Based on computations of ground state data of dihedral angles, it is concluded that *ortho-*, *meta-* and *para*-substituted isomers exhibit nearly planar molecular structures. Namely, C4-C2-C5-C3/C27-C23-C3-C5, C8-C6-C9-C7/C4-C27-C7-C9 and C6-C3-C7-C21/C15-C5-C21-C7 dihedral angle pairs are calculated as 175.85°/160.69°, 175.48°/177.79° and 175.96°/178.66°, respectively. On the other hand, other dihedral angle pairs mentioned in the Table 1 were determined between -0.04° and -0.65°. All bond parameters of the studied isomers were determined to be in good agreement with other similar structures reported as well as literature data [12, 37-39].

Table 1. Selected bond parameters for studied compounds

Bond Length (Å)	*o*-OH	Bond Length (Å)	*m*-OH	Bond Length (Å)	*p*-OH	Exp.
C2-O1	1.225	C6-O3	1.223	C3-O1	1.225	1.237[a]
C27-O28	1.363	C22-O1	1.367	C4-O2	1.363	1.361[a], 1.362[b] 1.354[c]
C2-C5	1.484	C6-C9	1.484	C3-C7	1.481	1.463[a]
C4-C12	1.402	C8-C16	1.402	C6-C11	1.402	1.398[a]
C4-C14	1.403	C8-C18	1.401	C6-C23	1.401	1.385[a]
C23-C27	1.414	C27-C4	1.401	C5-C15	1.404	1.386[a], 1.404[c]
Bond Angle (°)		**Bond Angle (°)**		**Bond Angle (°)**		
O1-C2-C5	121.09	O3-C6-C9	121.36	O1-C3-C7	121.57	120.40[a]
O1-C2-C4	119.99	O3-C6-C8	119.89	O1-C3-C6	119.72	119.33[a]
C27-C23-C3	120.43	C4-C27-C7	120.95	C15-C5-C21	119.87	120.22[a]
C3-C5-C2	120.12	C7-C9-C6	120.46	C21-C7-C3	120.40	122.63[a]
Dihedral Angle (°)		**Dihedral Angle (°)**		**Dihedral Angle (°)**		
C4-C2-C5-C3	175.85	C8-C6-C9-C7	175.48	C6-C3-C7-C21	175.96	168.96[a]
C27-C23-C3-C5	160.69	C4-C27-C7-C9	177.79	C15-C5-C21-C7	178.66	176.0[a]
C12-C4-C14-C19	-0.65	C16-C8-C18-C23	-0.02	C11-C6-C23-C25	-0.04	0.3[a]
C23-C27-C18-C16	-0.41	C27-C4-C22-C20	-0.1	C5-C15-C13-C4	-0.1	-2.3, 0.7[c]

[a] Ref. [35], [b] Ref. [36], [c] Ref. [37]

Thermodynamic Parameters

Table 2 demonstrates the calculated physicochemical and thermodynamic parameters of *o*-, *m*-, and *p*-substituted chalcone derivatives in both gas and solvent phases.

Table 2. Thermodynamic and physicochemical parameter estimations at B3LYP/6- 311++G (d, p) level

o-OH	Vacuum	ACN	DMSO	Water
DM (Debye)	3.329	4.726	4.747	4.774
ΔE (a.u.)	-729.212	-729.223	-729.223	-729.224
ΔH (a.u.)	-729.211	-729.222	-729.222	-729.223
ΔG (a.u.)	-729.269	-729.281	-729.282	-729.282
$\Delta E_{thermal}$ (kcal/mol)	152.084	151.993	151.992	151.991
$\Delta E_{vib.}$ (kcal/mol)	150.307	150.215	150.215	150.214
Cv (cal/molK)	55.511	55.586	55.586	55.586
$Cv_{vib.}$ (cal/molK)	49.549	49.624	49.624	49.624
S (cal/molK)	123.903	124.376	124.363	124.330
$S_{vib.}$ (cal/molK)	48.422	48.889	48.876	48.843
α (a.u.)	207.050	284.059	285.115	286.500
***m*-OH**	**Vacuum**	**ACN**	**DMSO**	**Water**
DM (Debye)	4.494	6.413	6.441	6.477
ΔE (a.u.)	-729.213	-729.226	-729.227	-729.227
ΔH (a.u.)	-729.212	-729.225	-729.226	-729.226
ΔG (a.u.)	-729.271	-729.284	-729.284	-729.285
$\Delta E_{thermal}$ (kcal/mol)	151.934	151.972	151.970	151.966
$\Delta E_{vib.}$ (kcal/mol)	150.157	150.195	150.192	150.189
Cv (cal/molK)	55.826	55.653	55.654	55.655
$Cv_{vib.}$ (cal/molK)	49.865	49.691	49.692	49.694
S (cal/molK)	124.825	123.667	123.689	123.720
$S_{vib.}$ (cal/molK)	49.296	48.137	48.158	48.190
α (a.u.)	205.930	281.408	282.465	283.854
***p*-OH**	**Vacuum**	**ACN**	**DMSO**	**Water**
DM (Debye)	2.907	4.456	4.478	4.506
ΔE (a.u.)	-729.214	-729.229	-729.229	-729.229
ΔH (a.u.)	-729.213	-729.228	-729.228	-729.228
ΔG (a.u.)	-729.272	-729.286	-729.287	-729.287
$\Delta E_{thermal}$ (kcal/mol)	152.013	151.951	151.949	151.945
$\Delta E_{vib.}$ (kcal/mol)	150.235	150.174	150.171	150.167
Cv (cal/molK)	55.655	55.534	55.536	55.538
$Cv_{vib.}$ (cal/molK)	49.694	49.572	49.574	49.577
S (cal/molK)	124.137	123.311	123.330	123.357
$S_{vib.}$ (cal/molK)	48.574	47.740	47.760	47.787
α (a.u.)	211.545	293.520	294.675	296.193

In the gas phase, the dipole moment and polarizability values of the isomers changed in the following order: DM (in Debye) 2.907 (*p*-) < 3.329 (*o*-) < 4.494 (*m*-) and α (in a.u.) 205.930 (*m*-) < 207.050 (*o*-) < 211.545 (*p*-). For both parameters, similar trends are observed in the solvent phase values. The highest polarizability value, 296.193 a.u., was obtained for the *para* isomer in the water phase. It can be expressed that *para* substitution on the aromatic ring makes the compound more polarizable. The gas phase total energy values for *o*-, *m*-, and *p*-OH derivatives were calculated as -729.212 a.u., -729.213 a.u., and -729.214 a.u., respectively. The change of substituent position did not create a significant difference in the enthalpy and free energy values, as well as in the total energy values. The highest heat capacity (Cv) and entropy (S) values were determined as 55.826 cal/molK and 124.825 cal/molK, respectively, in the gas phase for the *meta*-substituted derivative.

Vibrational Analysis

In literature reviews, no experimental FT-IR evaluation of the studied derivatives was found except *p*-substituted isomer. However, in the relevant study, only C=O and aromatic ring C-H stretching vibrations were mentioned for the *para* isomer [40]. Therefore, in this section, the vibrational analysis of all three isomers is discussed theoretically. The theoretically predicted FT-IR spectra of studied isomers are shown in Figure 5. Since molecular structures of studied isomers consist of 29 atoms, they reveal total 81 different vibrational modes according to the 3N-6 formula. The selected vibrational mode assignments for mentioned compounds are listed in Table 3.

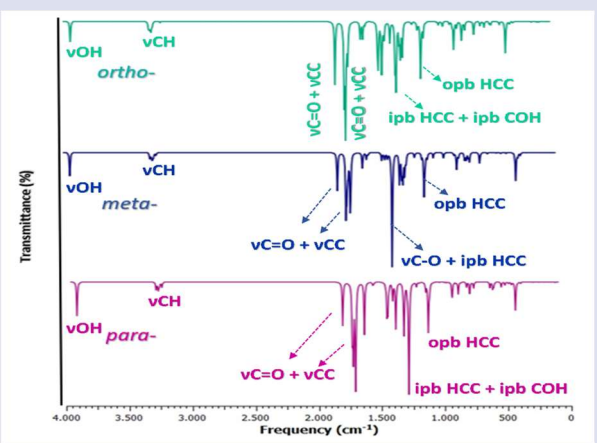

Figure 5. Theoretically simulated IR spectra of studied derivatives

FT-IR analysis facilitates the determination of the C=O stretching vibration band due to its specific region. νC=O stretching vibrations of *α,β*-unsaturated ketones are observed in the range of 1715-1680 cm^{-1} [41]. Herein, C=O stretching bands of *o*-, *m*-, and *p*- isomers were estimated in the range of 1560-1684 cm^{-1}, 1565-1690 cm^{-1} and 1561-1685 cm^{-1}, respectively. In the literature, the experimental carbonyl stretching vibration for the *p*-isomer has been reported as 1651 cm^{-1} [40]. νOH stretching vibrations are generally observed around 3500-3700 cm^{-1}. The calculated O-H stretching wavenumbers for the studied compounds were assigned at 3766 cm^{-1} (*o*-), 3769 cm^{-1} (*m*-) and 3763 cm^{-1} (*p*-) as pure mode. The theoretical νC-H (aromatic) bond stretching vibrations of studied isomers appeared at range of 3136-3151 cm^{-1} (*o*-), 3133-3149 cm^{-1} (*m*-), and 3128-3146 cm^{-1} (*p*-) as pure bonding vibrations with lower IR intensities. Also, the predicted peaks in regions 3110-3130 cm^{-1} (*o*-), 3100-3128 cm^{-1} (*m*-), and 3099-3124 cm^{-1} (*p*-) were assigned as C-H (aromatic) bond asymmetric stretching modes. The presence of the phenolic group has been indicated by a broad band at 3350 cm^{-1} for the *p*-isomer [40]. While C-H in-plane bending vibrations were calculated at 1548-1158 cm^{-1} region, out-of-plane bending vibrations were determined at 973-845 cm^{-1} region.

Table 3. The computed approximate frequencies (in cm^{-1}) for *o*-, *m*-, and *p*- isomers

	o-OH			*m*-OH			*p*-OH	
Assignment	**I_{IR}**	**Unscaled**	**Scaled**	**I_{IR}**	**Unscaled**	**Scaled**	**I_{IR}**	**Unscaled**	**Scaled**
νOH	56	3831	3766	86	3834	3769	124	3828	3763
νCH	13	3205	3151	15	3203	3149	11	3200	3146
νCH	11	3201	3147	11	3199	3145	17	3199	3145
νCH	8	3198	3144	1	3195	3141	1	3196	3142
νCH	2	3192	3138	6	3188	3134	5	3188	3134
νCH	14	3190	3136	5	3187	3133	25	3182	3128
ν_{as}CH	22	3184	3130	20	3182	3128	1	3178	3124
ν_{as}CH	4	3179	3125	9	3176	3122	9	3176	3122
ν_{as}CH	10	3174	3120	10	3172	3118	10	3172	3118
ν_{as}CH	0	3170	3116	0	3162	3108	0	3162	3108
ν_{as}CH	0	3164	3110	10	3154	3100	19	3153	3099
νCH	4	3111	3058	1	3149	3095	1	3144	3091
νC=O + νCC	173	1713	1684	138	1719	1690	158	1714	1685
νC=O + νCC	8	1652	1583	208	1651	1582	1	1654	1585
νC=O + νCC	204	1639	1570	126	1644	1575	185	1638	1569
νC=O + νCC	296	1628	1560	61	1634	1565	255	1629	1561
νCC + ipb HCC	86	1613	1545	167	1617	1549	75	1616	1548
νCC + ipb HCC	28	1610	1542	85	1613	1545	365	1610	1542
νCC + ipb HCC	2	1521	1457	56	1521	1457	190	1541	1476
νCC + ipb HCC	47	1512	1448	0	1520	1456	0	1520	1456
ipb HCC + ipb COH	46	1492	1429	25	1490	1427	10	1475	1413
νCC + ipb HCC	10	1476	1414	7	1475	1413	7	1467	1405
νC-O + ipb HCC	56	1276	1222	415	1285	1231	169	1291	1237
ipb HCC + ipb COH	170	1225	1174	78	1209	1158	185	1225	1174
Ph breathing + opb HCC	3	1016	973	2	1016	973	2	1016	973
opb HCC	0	960	920	10	962	922	0	969	928
opb HCC	10	888	851	11	882	845	2	886	849

Abbreviations; I_{IR}: IR intensity, ν: symmetric stretching, ν_{as}: asymmetric stretching, ipb: in plane bending, opb: out of plane bending,

FMO (Frontier Molecular Orbital) and MEP (Molecular Electrostatic Potential) Analyses

The outputs obtained from the analysis of frontier molecular orbitals provide valuable information about the distinct chemical characteristics of the molecule of interest by allowing the determination of chemical reactivity parameters. Herein, Table 4 represents the computed DFT-based reactivity parameters of studied isomers. HOMO and LUMO energy values were obtained from calculation outputs performed using density functional theory. The difference between HOMO and LUMO energies (ΔE) is an important merit in determining some properties of a molecule, such as its kinetic stability, chemical reactivity, and chemical hardness. In addition to gas phase, ACN, DMSO, and water phase calculations were also performed using the IEFPCM solvent model to peruse solvent effects. Accordingly, the energy gap values in the gas phase were calculated as: 4.013 eV (*m*-) > 3.898 eV (*p*-) > 3.832 eV (*o*-). For the solvent phases, the highest ΔE values were also obtained for the *meta*-substituted derivative as 3.835 eV (ACN) > 3.832 eV (DMSO) > 3.829 eV (water). The larger the energy gap value indicates lower chemical reactivity and higher kinetic stability. The same trend was followed in chemical hardness values, and the highest values were obtained for the *meta*- derivative: η, eV, 2.006 (vacuum) > 1.918 (ACN) > 1.916 (DMSO) > 1.915 (water). The electrophilicity index (ω) parameter describes the electrophilic power of the molecule. For all phases studied, the highest electrophilic index values were calculated for the *ortho*-substituted derivative as 5.689 eV (water) > 5.684 eV (DMSO) > 5.682 eV (ACN) > 5.431 eV (vacuum). Therefore, the *o*-OH derivative is expected to exhibit slightly more electrophilic character.

Table 4. The computed chemical reactivity parameters of studied isomers

o-OH	E_{HOMO}	E_{LUMO}	ΔE	η	μ	χ	ω	ω^+	ω^-	ΔN_{max}	ΔE_{back}
Vacuum	-6.478	-2.646	3.832	1.916	-4.562	4.562	5.431	3.390	7.9516	2.381	-0.479
ACN	-6.511	-2.743	3.768	1.884	-4.627	4.627	5.682	3.604	8.2308	2.456	-0.471
DMSO	-6.512	-2.744	3.768	1.884	-4.628	4.628	5.684	3.606	8.2338	2.456	-0.471
Water	-6.513	-2.746	3.767	1.884	-4.630	4.630	5.689	3.610	8.2397	2.458	-0.471
***m*-OH**	**E_{HOMO}**	**E_{LUMO}**	**ΔE**	**η**	**μ**	**χ**	**ω**	**ω^+**	**ω^-**	**ΔN_{max}**	**ΔE_{back}**
Vacuum	-6.531	-2.518	4.013	2.006	-4.525	4.525	5.104	3.092	7.617	2.256	-0.502
ACN	-6.545	-2.710	3.835	1.918	-4.628	4.628	5.584	3.510	8.137	2.413	-0.479
DMSO	-6.545	-2.713	3.832	1.916	-4.629	4.629	5.592	3.517	8.146	2.416	-0.479
Water	-6.546	-2.717	3.829	1.915	-4.632	4.632	5.602	3.526	8.157	2.419	-0.479
***p*-OH**	**E_{HOMO}**	**E_{LUMO}**	**ΔE**	**η**	**μ**	**χ**	**ω**	**ω^+**	**ω^-**	**ΔN_{max}**	**ΔE_{back}**
Vacuum	-6.281	-2.383	3.898	1.949	-4.332	4.332	4.814	2.892	7.224	2.223	-0.487
ACN	-6.307	-2.587	3.720	1.860	-4.447	4.447	5.316	3.325	7.772	2.391	-0.465
DMSO	-6.308	-2.589	3.719	1.860	-4.449	4.449	5.321	3.329	7.778	2.392	-0.465
Water	-6.309	-2.594	3.715	1.858	-4.452	4.452	5.334	3.340	7.792	2.397	-0.464

Besides, DOS (density of states) diagrams and 3D pictorial presentations of the HOMO & LUMO densities of studied isomers are introduced in Figures 6 and 7, respectively. Through DOS diagrams, the number of molecular orbitals of each isomer at different energy levels can be figured out. Based on Figure 7, it is evident that the HOMO and LUMO densities of all three isomers are quite similar to each other. While LUMOs are spread throughout the molecule, HOMOs are located on the remaining part except the unsubstituted phenyl group. LUMOs exhibit antibonding character. The red and green colors designate negative and positive lobes.

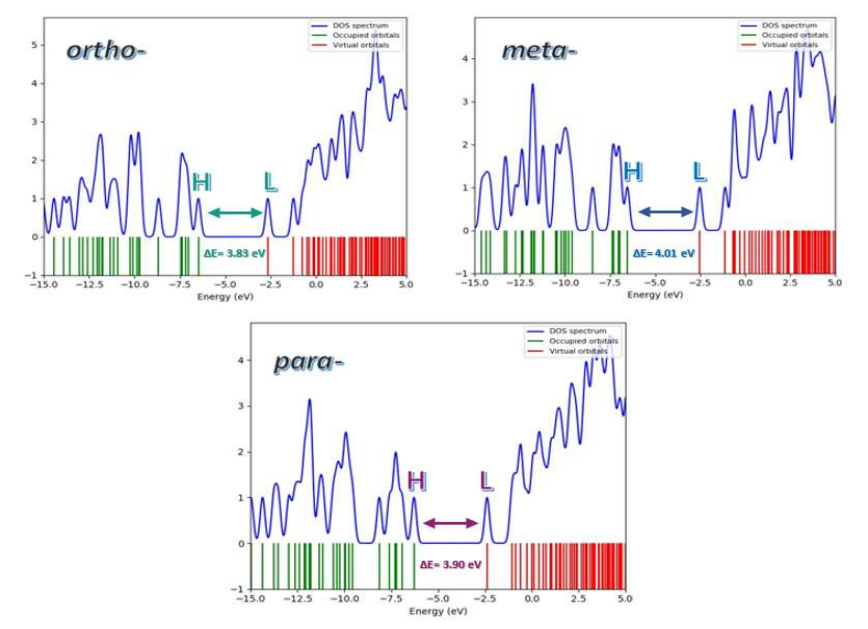

Figure 6. DOS diagrams of *o*-, *m*-, and *p*-substituted chalcone derivatives

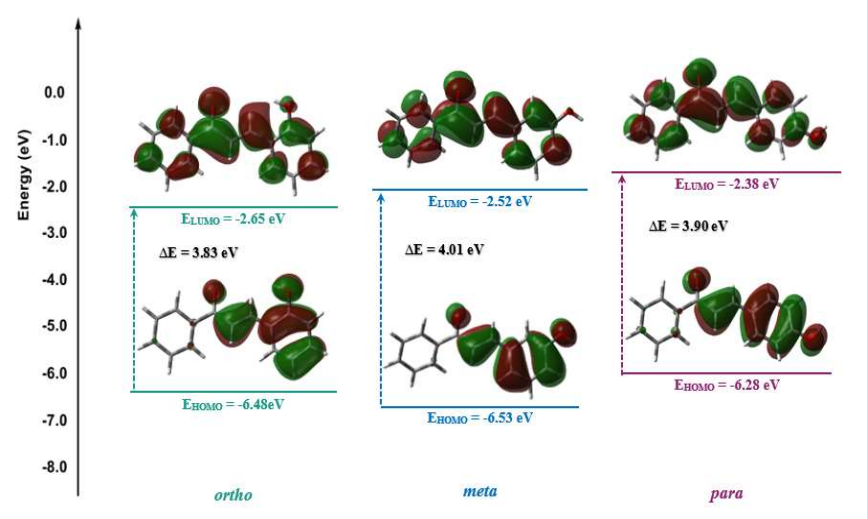

Figure 7. HOMO & LUMO densities (isoval: 0.02 a.u.) of studied isomers

The molecular electrostatic potential (MEP) mapping was put account to forecast the electrophilic and nucleophilic regions of OH-substituted isomers. Color codes are employed to easily understand the charge distribution [42]. Figure 8 displayed the MEP and ESP surfaces visualized at B3LYP/6-311++G (d, p) theory level. The potential values of MEP and ESP maps of studied isomers are in the range of -006705 a.u (deepest red) / +0.006705 a.u. (deepest blue) and -0.01286 a.u. (deepest red)/ 0.01286 a.u. (deepest blue). Accordingly, it is obvious that the electron density is higher around aromatic rings (because of π-electron cloud) and oxygen atoms, and there is predominantly red coloration (V<0). Apart from, blue coloration (V>0) is mostly observed around hydrogen atoms.

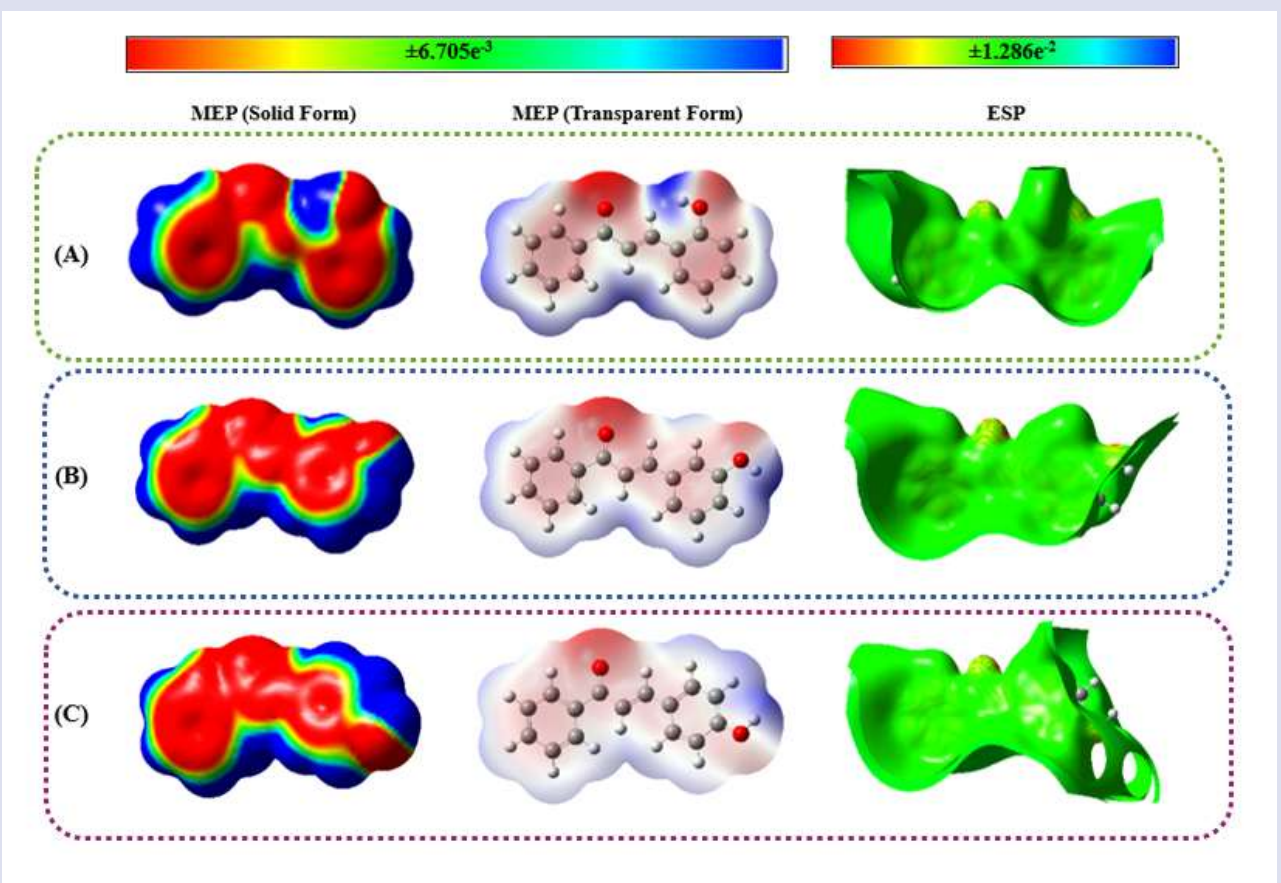

Figure 8. MEP and ESP maps of *o*-OH (A), *m*-OH (B), and *p*-OH (C) substituted derivatives

UV-vis Characterization

The absorption wavelengths of the studied chalcone derivatives were determined by performing TD-DFT calculations in the ACN, DMSO and water phases using the IEFPCM solvent model. Table 5 summarizes possible electronic transitions with relevant data. It is observed for each isomer that the absorption peak values are not significantly affected by the solvent environment. For all three compounds, the studied solvents revealed three distinct wavelengths and oscillator strengths. For *ortho*-OH derivative, water phase wavelengths were computed as 376.91 nm, 325.36 nm, and 288.35 nm, with oscillator strengths (*f*) of 0.3821, 0.3645, and 0.1041, in that order. In ACN and DMSO phases, the wavelengths of the obtained peaks were 377.03/325.32/288.39 nm and 377.94/325.93/288.80 nm, respectively. It has been determined that the following transitions contribute to the transitions with wavelengths 376.91/325.36/288.35 nm: HOMO-4→LUMO (20%), HOMO→LUMO (66%), HOMO-1→LUMO (66%), HOMO-4→LUMO (52%), HOMO-3→LUMO (34%). It can be seen from Table 5 that the same orbitals contribute to the electronic transitions in acetonitrile and DMSO environments. Although the calculated wavelengths for *meta*-OH and *para*-OH substituted derivatives differed relatively, similar electronic transitions were observed. In the literature review, experimental UV-vis results were found only for *ortho*- and *para*- derivatives. While the λ_{max} value was reported as 345 nm for the *ortho*- derivative [43], it was recorded as 395 nm for the *para*- derivative [44]. Additionally, for the *ortho*- derivative, plots of the orbitals contributing to electronic transitions in the DMSO phase are shown in Figure 9. With respect to Figure 9, absorption wavelengths can be qualified as π→π* and n→π* transition type.

Table 5. The computed λ_{max}, ΔE, and oscillator strength values of studied isomers in different solvent phases

	Medium	Symmetry	$\lambda_{calc.}$ (nm)	ΔE (eV)	*f*	Major Contributions
ortho-OH	Water	Singlet-A	376.91	3.2895	0.3821	H-4→L (20%), H→L (66%)
		Singlet-A	325.36	3.8106	0.3645	H-1→L (66%)
		Singlet-A	288.35	4.2998	0.1041	H-4→L (52%), H-3→L (34%)
	ACN	Singlet-A	377.03	3.2885	0.3806	H-4→L (20%), H→L (65%)
		Singlet-A	325.32	3.8112	0.3637	H-1→L (66%)
		Singlet-A	288.39	4.2992	0.1045	H-4→L (53%), H-3→L (33%)
	DMSO	Singlet-A	377.94	3.2805	0.4027	H-4→L (19%), H→L (66%)
		Singlet-A	325.93	3.8040	0.3614	H-1→L (66%)
		Singlet-A	288.80	4.2931	0.1086	H-4→L (53%), H-3→L (33%)
	Medium	**Symmetry**	**$\lambda_{calc.}$ (nm)**	**ΔE (eV)**	***f***	**Major Contributions**
meta-OH	Water	Singlet-A	366.28	3.3850	0.1357	H→L (53%), H-2→L (31%)
		Singlet-A	324.04	3.8262	0.6309	H-1→L (68%)
		Singlet-A	287.00	4.3201	0.0807	H-4→L (55%), H-3→L (30%)
	ACN	Singlet-A	366.36	3.3842	0.1045	H→L (47%), H-2→L (36%)
		Singlet-A	323.93	3.8275	0.6307	H-1→L (68%)
		Singlet-A	286.99	4.3202	0.0809	H-4→L (56%), H-3→L (28%)
	DMSO	Singlet-A	366.71	3.3810	0.1498	H→L (54%), H-2→L (30%)
		Singlet-A	324.84	3.8168	0.6334	H-1→L (68%)
		Singlet-A	287.41	4.3138	0.0843	H-4→L (55%), H-3→L (29%)
	Medium	**Symmetry**	**$\lambda_{calc.}$ (nm)**	**ΔE (eV)**	***f***	**Major Contributions**
para-OH	Water	Singlet-A	364.56	3.4009	0.7226	H→L (66%)
		Singlet-A	358.82	3.4553	0.1251	H-1→L (55%), H-3→L (29%)
		Singlet-A	282.97	4.3816	0.1539	H-3→L (61%), H-1→L (26%)
	ACN	Singlet-A	364.51	3.4014	0.6988	H→L (65%)
		Singlet-A	359.22	3.4515	0.1510	H-1→L (54%), H-3→L (27%)
		Singlet-A	282.98	4.3814	0.1538	H-3→L (62%), H-1→L (26%)
	DMSO	Singlet-A	365.99	3.3877	0.7705	H→L (68%)
		Singlet-A	359.25	3.4512	0.0944	H-1→L (56%), H-3→L (29%)
		Singlet-A	283.38	4.3752	0.1585	H-3→L (61%), H-1→L (26%)

H = HOMO; L = LUMO

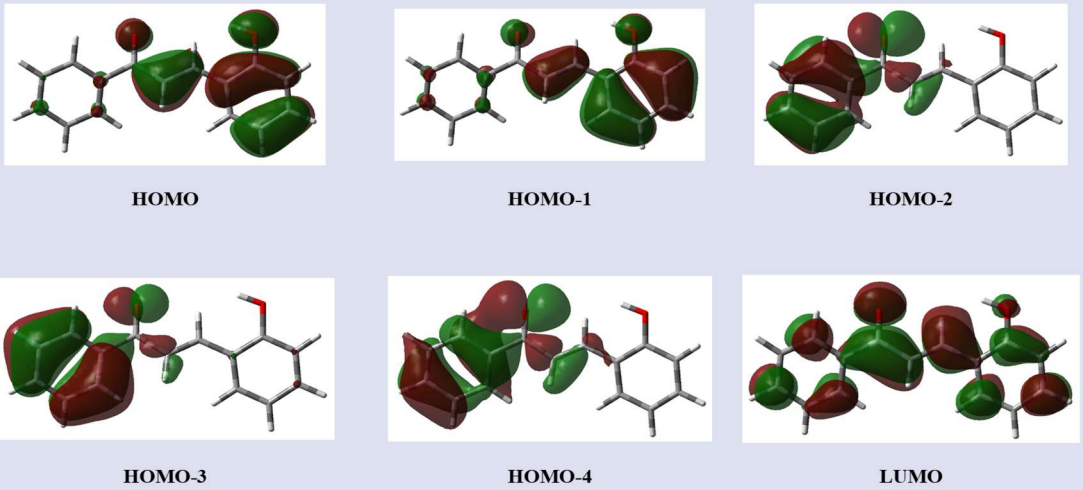

Figure 9. FMO plots contributing to the electronic transitions of *o*-OH isomer in DMSO

NBO Analysis

NBO theory analysis of a particular molecule provides an exhaustive insight into the electron density delocalization from Lewis's donor to non-Lewis's acceptor NBOs. In order to peruse all possible intramolecular interactions of mentioned isomers, the stabilization energy values were computed using the 2nd-order perturbation theory. The findings obtained are listed in Table 6. Interactions with a stabilization energy value of 10 kcal/mol and above were taken into account. As expected, the types of interactions (π → π*, LP → σ* and LP → π*) and energy values are quite close for all three isomers. Some different interactions were determined for the *o*-, *m*-, and *p*-substituted isomers, with energy values ranging from 9.99-28.77, 12.06-26.58, and 11.62-28.67 kcal/mol, respectively. The intramolecular hyperconjugative interactions were observed between π (C-C) and π* (C-C) bond orbitals and this generated intramolecular charge transfers that resulted in the stabilization of the studied molecules. Moreover,

according to Table 6, it can be concluded that the lone electron pairs (LP) existing on oxygen atoms are involved in intramolecular interactions and largely participate in the stabilization of all three isomers. Namely, for the *o*-OH isomer, the stabilization energies of the LP (2) O1(ED_i = 1.88793e) → σ* C2-C4 (ED_j = 0.06445e), LP (2) O1(ED_i = 1.88793e) → σ* C2-C5 (ED_j = 0.05825e), and LP (2) O28 (ED_i =1.86528e) → π* C23-C27 (ED_j = 0.42508e) transitions were calculated as 18.65, 18.69, and 28.77 kcal/mol, respectively. On the other hand, while the energies corresponding to LP → σ* transitions in *m*-OH and *p*-OH derivatives were calculated as 18.88, 18.02 kcal/mol and 18.96, 18.55 kcal/mol, respectively, the stabilization energy values of LP → π* interactions were determined as 26.58 and 28.67 kcal/mol.

Table 6. NBO analysis results of possible interactions for *o*-, *m*-, and *p*-substituted isomers

***o*-OH**	**Donor(i)**	**ED_i/e**	**Acceptor(j)**	**ED_j/e**	**$E^{(2)}$ kcal/mol**	**E(j)-E(i)/a.u**	**F(i.j)/a.u**
	π C3-C5	1.84726	π* O1-C2	0.20829	19.96	0.30	0.070
			π* C23-C27	0.42508	9.99	0.30	0.052
	π C10-C21	1.70219	π* C16-C18	0.31525	21.40	0.29	0.070
			π* C23-C27	0.42508	16.30	0.28	0.062
	π C14-C19	1.65123	π* C4-C12	0.36761	19.46	0.28	0.066
			π* C6-C8	0.32176	21.73	0.28	0.070
	π C16-C18	1.69247	π* C10-C21	0.30386	16.88	0.29	0.062
			π* C23-C27	0.42508	22.73	0.28	0.073
	π C23-C27	1.60589	π* C3-C5	0.11620	16.21	0.29	0.066
			π* C10-C21	0.30386	21.02	0.29	0.071
			π* C16-C18	0.31525	15.88	0.29	0.062
	LP (2) O1	1.88793	σ* C2-C4	0.06445	18.65	0.69	0.103
			σ* C2-C5	0.05825	18.69	0.70	0.103
	LP (2) O28	1.86528	π* C23-C27	0.42508	28.77	0.35	0.097
***m*-OH**	**Donor(i)**	**ED_i/e**	**Acceptor(j)**	**ED_j/e**	**$E^{(2)}$ kcal/mol**	**E(j)-E(i)/a.u**	**F(i.j)/a.u**
	π C4-C27	1.97110	π* C7-C9	0.10068	16.25	0.29	0.066
			π* C14-C25	0.31180	17.16	0.28	0.063
			π* C20-C22	0.38293	22.08	0.28	0.071
	π C7-C9	1.83860	π* O3-C6	0.20097	20.35	0.30	0.070
			π* C4-C27	0.37425	12.06	0.30	0.057
	π C8-C18	1.63947	π* O3-C6	0.20097	17.22	0.28	0.064
			π* C10-C23	0.32298	19.02	0.28	0.066
			π* C12-C16	0.28689	19.45	0.29	0.068
	π C10-C23	1.65314	π* C8-C18	0.36581	21.46	0.28	0.070
			π* C12-C16	0.28689	17.77	0.29	0.065
	π C12-C16	1.65158	π* C8-C18	0.36581	19.50	0.28	0.066
			π* C10-C23	0.32298	21.69	0.28	0.070
	π C14-C25	1.69361	π* C4-C27	0.37425	20.61	0.29	0.070
			π* C20-C22	0.38293	16.77	0.29	0.063
	π C20-C22	1.65027	π* C4-C27	0.37425	17.08	0.30	0.064
			π* C14-C25	0.31180	21.22	0.30	0.072
	LP (2) O1	1.87841	π* C20-C22	0.38293	26.58	0.36	0.094
	LP (2) O3	1.88822	σ* C6-C8	0.06548	18.88	0.69	0.103
			σ* C6-C9	0.05888	18.02	0.70	0.102
***p*-OH**	**Donor(i)**	**ED_i/e**	**Acceptor(j)**	**ED_j/e**	**$E^{(2)}$ kcal/mol**	**E(j)-E(i)/a.u**	**F(i.j)/a.u**
	π C4-C13	1.64301	π* C5-C15	0.38628	23.27	0.30	0.075
			π* C9-C19	0.28792	15.07	0.30	0.061
	π C5-C15	1.62414	π* C4-C13	0.38565	18.38	0.27	0.062
			π* C7-C21	0.12120	18.26	0.30	0.070
			π* C9-C19	0.28792	20.84	0.28	0.070
	π C6-C23	1.63948	π* O1-C3	0.21011	17.08	0.28	0.064
			π* C11-C27	0.28864	19.49	0.29	0.068
			π* C17-C25	0.32442	19.22	0.28	0.066
	π C7-C21	1.83728	π* O1-C3	0.21011	21.06	0.30	0.071
			π* C5-C15	0.38628	11.52	0.29	0.055
	π C9-C19	1.71275	π* C4-C13	0.38565	22.37	0.28	0.072
			π* C5-C15	0.38628	16.14	0.29	0.063
	π C11-C27	1.65204	π* C6-C23	0.36458	21.80	0.25	0.066
			π* C17-C25	0.32442	24.32	0.25	0.070
	π C17-C25	1.65433	π* C6-C23	0.36458	23.89	0.25	0.070
			π* C11-C27	0.28864	19.96	0.26	0.065
	LP 2 (O1)	1.88850	σ* C3-C6	0.06564	18.96	0.69	0.103
			σ* C3-C7	0.05800	18.55	0.69	0.103
	LP 2 (O2)	1.86766	π* C4-C13	0.38565	28.67	0.35	0.096

Conclusion

This paper presents the main findings of quantum chemical calculations performed on *ortho*-, *meta*- and *para*-substituted chalcones in order to study the effect of substitution position on molecular properties. The bond parameters of the DFT-optimized structures of the relevant isomers were compared with the data available in the literature, and the vibrational allocations of the frequencies were performed by creating theoretical FT-IR spectra. It was observed that the substitution positions of the studied OH-substituted chalcones affected their physicochemical properties and reactivity parameters. With a polarizability value of 296.193 a.u., it was determined that the *para* substitution on the aromatic ring made the molecule more polarizable. However, substituent position variation did not create a considerable distinction in the enthalpy, total energy, and free energy values. Considering the energy gap values, which are an important measure in FMO calculations, the highest values for both vacuum and solvent phases were obtained for the *meta* isomer. Accordingly, in gas phase the chemical reactivity order is predicted as *m*-OH < *p*-OH < *o*-OH. According to results of excited state calculations for the isomers, *ortho*-OH derivative exhibited maximum absorption at 378 nm, while energy required for predominant HOMO → LUMO electronic transition was computed as 3.2805 eV. As a result of *meta*- and *para*-substitution, the λ_{max} value was detected to shift towards slightly lower wavelengths, such as 366.71 and 365.99 nm, respectively. Natural bond orbital analysis was performed to peruse the stabilization energies of various intramolecular interactions of the studied isomers. It is anticipated that the findings obtained in the present study will provide the data needed for future studies. Also, the research outcomes are significant in terms of providing new insights into the effects of the substitution position.

Acknowledgement

The numerical calculations reported in this paper were fully performed at TUBITAK ULAKBIM, High Performance and Grid Computing Center (TRUBA resources).

Conflicts of interests

There are no conflicts of interest in this work.

References

[1] Narwal S., Devi B., Dhanda T., Kumar S. and Tahlan S., Exploring Chalcone Derivatives: Synthesis and Their Therapeutic Potential, *J. Mol. Struct.,* 1303 (2024) 137554.

[2] Yadav P., Lal K., Kumar A., Guru S.K., Jaglan S., Bhushan S., Green Synthesis and Anticancer Potential of Chalcone Linked-1,2,3-triazoles, *Eur. J. Med. Chem.*, 126 (2017) 944-953.

[3] Wang G., Xue Y., An L., Zheng Y., Dou Y., Zhang L., Liu Y., Theoretical Study on the Structural and Antioxidant Properties of Some Recently Synthesized 2,4,5-trimethoxy Chalcones, *Food Chem.*, 171 (2015) 89-97.

[4] Reddy M.V.B., Hung H.Y., Kuo P.C., Huang G.J., Chan Y.Y., Huang S.C., Wu S.J., Morris-Natschke S.L., Lee K.H. and Wu T.S., Synthesis and Biological Evaluation of Chalcone, Dihydrochalcone, and 1,3-diarylpropane Analogs as Anti-inflammatory Agents, *Bioorg. Med. Chem. Lett.*, 27(7) (2017) 1547-1550.

[5] Sharma C.S., Shekhawat K.S., Chauhan C.S., Kumar N., Synthesis and Anticonvulsant Activity of Some Chalcone Derivatives, *J. Chem. Pharm. Res*., 5(10) (2013) 450-454.

[6] Parikh K., Joshi D., Antibacterial and Antifungal Screening of Newly Synthesized Benzimidazole-Clubbed Chalcone Derivatives, *Med. Chem. Res.,* 22(8) (2013) 3688-3697.

[7] Abbo H.S., Lai C.H., Titinchi S.J.J., Substituent and Solvent Effects on UV-visible Absorption Spectra of Chalcones Derivatives: Experimental and Computational Studies, *Spectrochim. Acta A Mol. Biomol. Spectrosc.,* 303 (2023) 123180.

[8] Ma L., Yang Z., Li C., Zhu Z., Shen X.,Hu L., Design, Synthesis and SAR Study of Hydroxychalcone Inhibitors of Human β-secretase (BACE1), *J. Enzyme Inhib. Med. Chem*., 26(5) (2011) 643–648.

[9] Cyboran-Mikołajczyk S., Matczak K., Olchowik-Grabarek E., Sękowski S., Nowicka P., Krawczyk-Łebek A., Kostrzewa-Susłow E., The Influence of the Chlorine Atom on the Biological Activity of 2'-hydroxychalcone in Relation to the Lipid Phase of Biological Membranes - Anticancer and Antimicrobial Activity, *Chem. Biol. Interact.,* 398 (2024) 111082.

[10] Patil P., Zangade S., Synthesis and Comparative Study of Cytotoxicity and Anticancer Activity of Chalconoid-Co(II) Metal Complexes with 2-hydroxychalcones Analogue Containing Naphthalene Moiety, *J. Indian Chem. Soc.***,** 99 (2022) 100274.

[11] Bronikowska J., Kłosek M., Janeczko T., Kostrzewa-Susłow E., Czuba Z.P., The Modulating Effect of Methoxy-Derivatives of 2'-hydroxychalcones on the Release of IL-8, MIF, VCAM-1 and ICAM-1 by Colon Cancer Cells, *Biomed. Pharmacother.,* 145 (2022) 112428.

[12] Wilhelm A., Bonnet S.L., Twigge L., Rarova L., Stenclova T., Visser H.G., Schutte-Smith M., Synthesis, Characterization and Cytotoxic Evaluation of Chalcone Derivatives, *J. Mol. Struct.,* 1251 (2022) 132001.

[13] Sahib M.A., Mahdi M.F., Molecular Docking, Synthesis, Characterization and Preliminary Evaluation of some New 3-Ethyl-1H-Indole Derivatives as Potential COX-2 Inhibitors, *Adv. J. Chem. A*, 8(5) (2025) 948-960.

[14] Sandeli A.E., Khiri-Meribout N., Benzerka S., Boulebd H., Gürbüz N., Özdemir N., Özdemir I., Synthesis, Structures, DFT Calculations, and Catalytic Application in the Direct Arylation of Five-Membered Heteroarenes with Aryl Bromides of Novel Palladium-N-Heterocyclic Carbene PEPPSI-Type Complexes, *New J. Chem.***,** 45 (2021) 17878-17892.

[15] Frisch M.J., Trucks G.W., Schlegel H.B., Scuseria G.E. et.al. (2016). Gaussian 16 Rev. B.01, Wallingford, CT.

[16] Lee C., Yang W. and Parr R.G., Development of the Colle-Salvetti Correlation-Energy Formula into a Functional of the Electron Density, *Phys. Rev. B.,* 37 (1988) 785–789.

[17] Becke A.D., A New Mixing of Hartree–Fock and Local Density-Functional Theories, *J. Chem. Phys.,* 98 (1993) 1372–1377.

[18] Becke A.D., Density-Functional Thermochemistry. III. The Role of Exact Exchange, *J. Chem. Phys.,* 98 (1993) 5648–5652.

[19] Dennington R., Keith T.A., Millam J.M., GaussView, Version 6 Semichem Inc., Shawnee Mission, KS 2016.

[20] O'Boyle N.M., Tenderholt A.L., Langer K.M.J., cclib: A Library for Package-Independent Computational Chemistry Algorithms, *Comp. Chem*., 29 (2008) 839.

[21] Tomasi J., Mennucci B., Cammi R., Quantum Mechanical Continuum Solvation Models, *Chem. Rev.*, 105 (2005) 2999–3093.

[22] Casida M.E., Jamorski C., Casida K.C., Salahub D.R., Molecular Excitation Energies to High-Lying Bound States from Time-Dependent Density-Functional Response Theory: Characterization and Correction of the Time-Dependent Local Density Approximation Ionization Threshold, *J. Chem. Phys*., 108 (1998) 4439–4449.

[23] McQuarrie D.A., Statistical Thermodynamics, Harper & Row Publishers, New York, 1973.

[24] Herzberg G., Molecular Spectra and Molecular Structure III, 1. Edition, D. Van Nostrand Company, Inc., New York, 1964.

[25] Serdaroğlu G., Durmaz S., DFT and statistical mechanics entropy calculations of diatomic and polyatomic molecules, *Indian J. Chem*., 49 (2010) 861-866.

[26] Koopmans T., Über die zuordnung von wellenfunktionen und eigenwerten zu den einzelnen elektronen eines atoms, *Physica* 1–6 (1934) 104–113.

[27] Parr R.G., Electrophilicity Index, *J. Am. Chem. Soc.,* 121 (1999) 1922-1924.

[28] Parr R.G., Pearson R.G., Absolute Hardness: Companion Parameter to Absolute Electronegativity, *J. Am. Chem. Soc.*, 105 (1983) 7512-7516.

[29] Pearson R.G., Absolute Electronegativity and Hardness Correlated with Molecular Orbital Theory, *Proc. Natl. Acad. Sci. U.S.A,* 83 (1986) 8440-8441.

[30] Perdew J.P. and Levy M., Physical Content of the Exact Kohn-Sham Orbital Energies: Band Gaps and Derivative Discontinuities, *Phys. Rev. Let.*, 51 (1983) 1884-1887.

[31] Perdew J.P., Parr R.G., Levy M. and Balduz J.L, Density-Functional Theory for Fractional Particle Number: Derivative Discontinuities of the Energy, *Phys. Rev. Let.,* 49 (1982) 1691.

[32] Gazquez J.L., Cedillo A. and Vela A., Electrodonating and Electroaccepting Powers, *J. Phys. Chem. A.*, 111(10) (2007) 1966-1970.

[33] Gomez B., Likhanova N.V., Domínguez-Aguilar M.A., Martínez-Palou R., Vela A. and Gazquez J.L., Quantum Chemical Study of the Inhibitive Properties of 2-Pyridyl-azoles, *J. Phys. Chem. B.,* 110(18) (2006) 8928-8934.

[34] Weinhold F., Landis C.R., Glendening E.D., What Is NBO Analysis and How Is It Useful? *Int. Rev. Phys. Chem.*, 35 (2016) 399-440.

[35] Reed A.E., Curtiss L.A. and Weinhold F., Intermolecular Interactions from a Natural Bond Orbital, Donor-Acceptor Viewpoint, *Chem. Rev.* 88(6) (1988) 899-926.

[36] Sahib M.A., Mahdi M.F., Identification of Indole Derivatives as Selective Cyclooxygenase-2 Inhibitors by Virtual Screening and Molecular Dynamic Simulation, *Turkish Comp. Theo. Chem. (TC&TC),* 9(2) (2025) 19-32.

[37] Qiu X.Y., Yang S.L., Liu W.S. and Zhu H.L., (E)-3-(4-hydroxyphenyl)-1-(4-methoxyphenyl) prop-2-en-1-one, *Acta Cryst.* E62 (2006) 3324-3325.

[38] Paixão J.A., Beja A.M., Silva M.R., Alte da Veiga L., Serra A.C., 3-Hydroxybenzaldehyde, *Acta Cryst.* C56 (2000) 1348-1350.

[39] Jasinski J.P., Butcher R.J., Narayana B., Swamy M.T., Yathirajan H.S., Redetermination of 4-hydroxybenzaldehyde, *Acta Cryst*. E64 (2008) o187.

[40] Shubhalaxmi, Hahne S., Zschille C., Jayarama A., Bhat K.S., Crystal Structure Studies and Thermal Characterization of Novel 4-hydroxychalcone Derivative, *Chem. Sci. Trans*., 2(3) (2013) 841-846.

[41] Prasad A.A., Muthu K., Meenatchi V., Rajasekar M., Agilandeshwari R., Meena K., Manonmoni J.V., Meenakshisundaram S.P., *Spectrochim. Acta A Mol. Biomol. Spectrosc.* 140 (2015) 311–327.

[42] Murray J.S., Sen K., Molecular Electrostatic Potentials: Concepts and Applications, first ed., Elsevier, (Amsterdam, 1996).

[43] Turowska-Tyrk I., Grzesniak K., Trzop E., Zych T., Monitoring Structural Transformations in Crystals. Part 4. Monitoring Structural Changes in Crystals of Pyridine Analogs of Chalcone During [2+2]-Photodimerization and Possibilities of the Reaction in Hydroxy Derivatives, *J. Solid State Chem*., 174 (2003) 459–465.

[44] Tomečková V., Guzy J., Kušnír J., Fodor K., Mareková M., Chavková Z., Perjési P., Comparison of the Effects of Selected Chalcones, Dihydrochalcones and Some Cyclic Flavonoids on Mitochondrial Outer Membrane Determined by Fluorescence Spectroscopy, *J. Biochem. Biophys. Methods*, 69 (2006) 143–150.